Volume 7 | Number 19 | 21 May 2019 | Pages 5509–5842

Journal of Materials Chemistry C

Materials for optical, magnetic and electronic devices

rsc.li/materials-c

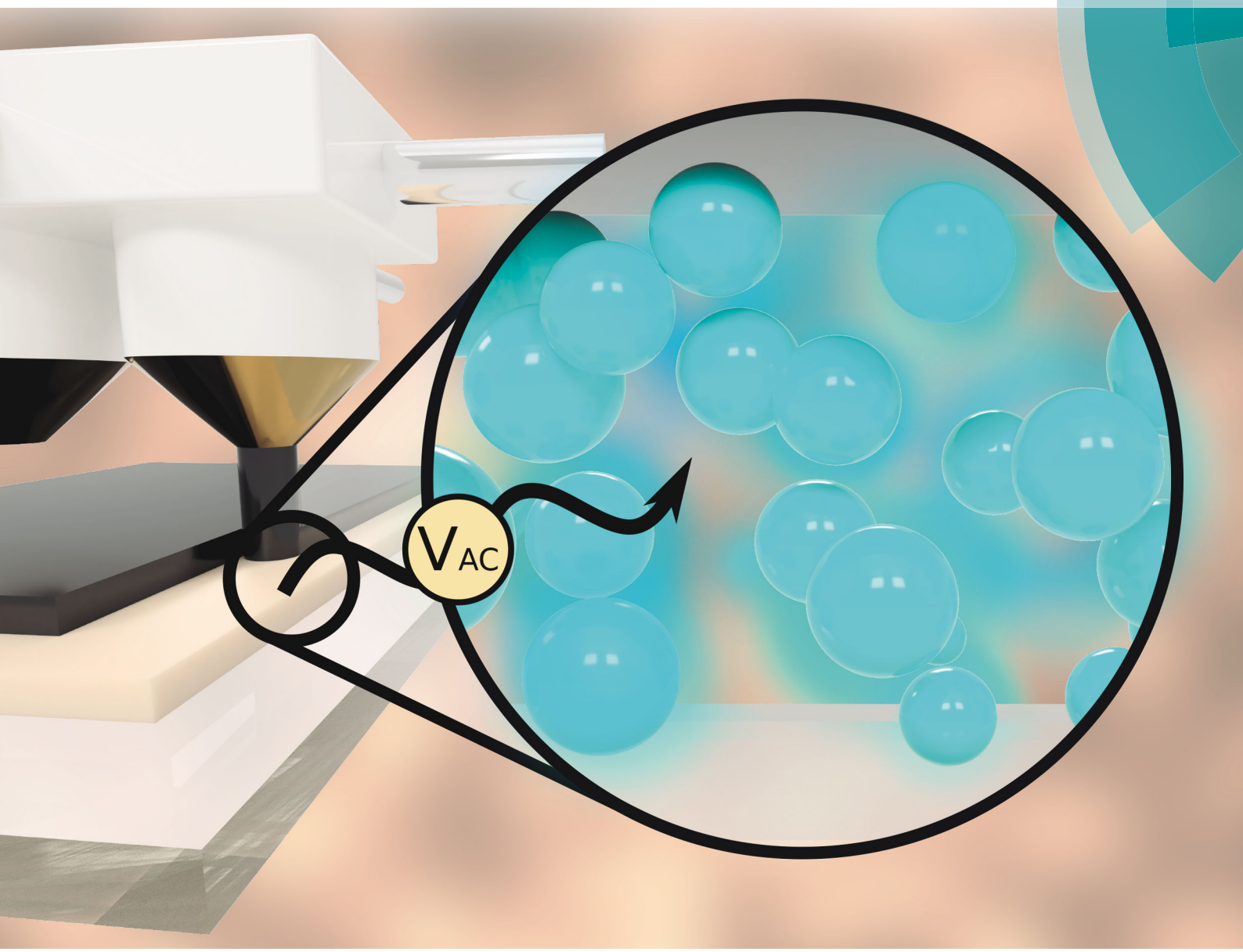

ISSN 2050-7526

ROYAL SOCIETY OF CHEMISTRY | Celebrating IYPT 2019

COMMUNICATION

G. Kane Jennings, Douglas E. Adams *et al.*

3D-Printed alternating current electroluminescent devices

Journal of Materials Chemistry C

COMMUNICATION

View Article Online
View Journal | View Issue

Cite this: J. Mater. Chem. C, 2019, 7, 5573

Received 31st January 2019,
Accepted 22nd March 2019

DOI: 10.1039/c9tc00619b

rsc.li/materials-c

3D-Printed alternating current electroluminescent devices†

Cole D. Brubaker,[a] Kailey N. Newcome,[a] G. Kane Jennings *[b] and Douglas E. Adams *[ac]

This work explores the use of metal-doped zinc sulfide (ZnS) phosphor materials by harnessing their unique optical response for the development of 3D-printed electroluminescent devices. Through materials design and processing considerations, the ability to manufacture alternating current electroluminescent (ACEL) devices using commercially available fused deposition modeling (FDM) type 3D printing systems is demonstrated. ZnS-based phosphors are incorporated within a polylactic acid (PLA) host matrix and fabricated by depositing a single layer (100 μm) of PLA/phosphor-functionalized filament onto an ITO-coated glass slide, sandwiched between a second electrode comprising of 3D-printed carbon-doped conductive PLA. By applying a voltage across the PLA/phosphor layer, 3D-printed ACEL devices display a tunable bright blue/green luminescent behavior. The observed optical response is highly reproducible and dependent on both the applied voltage and frequency of excitation, where the recorded emission displays a significant blue shift with increasing excitation frequencies. ACEL devices with various geometric shapes are printed to further demonstrate the effectiveness and feasibility of additive manufacturing and 3D printing technologies as an additional methodology and approach for developing custom light emitting devices and displays.

Introduction

With applications ranging from lighting and displays[1,2] to wearable devices[3–5] and even structural health monitoring[6] and visual sensing,[7] metal-doped phosphor systems have received significant interest from the research community due to their tunable response and behavior. Owing to their underlying composition and structure, luminescent phosphor materials capable of emitting colors across the visible spectrum have been developed.[8,9] Traditionally incorporated within a polymer host matrix or binder, both electroluminescent (EL) and mechanoluminescent (ML) devices and structures capable of optically responding to electrical and mechanical stimuli, respectively, have been demonstrated using a variety of metal-doped phosphor systems. ZnS-based phosphors are among the most commonly studied phosphors for device fabrication due to their intense luminescent and emissive properties, as well as their overall temporal durability and stability.[10–12] Transition metal ions, including copper[10–13] and manganese,[12–15] among others, are examples of dopants that have been used to modulate the optical response and emissive behavior of ZnS-based phosphor materials. In each case, the metal ions substituted within the host crystal lattice results in the formation of discrete energy levels that are responsible for the observed differences in the luminescent and emissive behaviors for the various metal ion dopants.

As a result of their customizable optical properties and multi-stimuli responsive behavior, ZnS-based phosphors have been increasingly used in the development of alternating current electroluminescent (ACEL) devices. In their most basic configuration, ACEL devices are comprised of a phosphor/dielectric composite binder and a set of conductive electrodes through which external electrical stimuli can be applied to the device. The subsequent voltage drop across the phosphor/dielectric layer under electrical excitation results in an intense, bright luminescence based on the specific type of embedded phosphor and the applied voltage. Such devices have been used for a range of applications related to lighting and displays, and are continuing to gain attention for additional uses, such as sensing,[16] due to the flexibility of their design and implementation. Traditionally ACEL devices are fabricated in multi-step processes involving various spin coating, masking, drop casting and curing iterations to manufacture the final device. Polymer host matrices such as polydimethyl siloxane (PDMS),[10–13,17,18] and other thermoplastics,[14] resins[1,16,19] and epoxies[20–22] have all been reported as encapsulating agents for the development

[a] Department of Civil and Environmental Engineering, Vanderbilt University, Nashville, Tennessee 37235, USA. E-mail: douglas.adams@vanderbilt.edu
[b] Department of Chemical and Biomolecular Engineering, Vanderbilt University, Nashville, Tennessee, 37235, USA. E-mail: kane.g.jennings@vanderbilt.edu
[c] Department of Mechanical Engineering, Vanderbilt University, Nashville, Tennessee 37235, USA

† Electronic supplementary information (ESI) available. See DOI: 10.1039/c9tc00619b

of both the phosphor/dielectric composite and conducting electrodes. Although such conventional manufacturing approaches have resulted in the demonstration of a number of functional and durable ACEL devices, these fabrication techniques are often time-consuming when manufacturing single devices or small arrays, posing a challenge to the more widespread use and implementation of ACEL devices.

In order to address such constraints, we herein report the first known demonstration of a 3D-printed ACEL device using a commercially available fused deposition modeling (FDM) type 3D printing system. Utilizing a thermoplastic-based feedstock, parts and structures with complex and varied geometries can be rapidly manufactured in a layer-by-layer fashion without the need for any post processing or additional curing steps. As opposed to conventional manufacturing techniques that often require one or more hours of fabrication time,[10,13] individual ACEL devices with functional and customizable responses can be printed in a matter of minutes using the approach discussed in this paper. Building upon recent reports in which phosphors have been utilized for direct ink writing (DIW) processes,[23] our 3D-printed device consists of a polylactic acid (PLA)-based phosphor/dielectric composite binder sandwiched between an indium tin oxide (ITO) glass substrate and a 3D-printed carbon-based conductive PLA electrode to achieve device illumination and luminescence. PLA was selected as the host matrix for the development of our ACEL devices due to its minimal optical contributions in the visible range, ease of materials processing, compatibility with FDM-type 3D-printing systems, and lack of requirements for additional curing agents during the manufacturing and printing process. 3D-Printed PLA/phosphor ACEL devices were tested under various electrical configurations, and the resulting optical responses were recorded. By embedding copper-doped ZnS phosphors (ZnS:Cu, with an approximate particle size of 24 ± 6 μm, Fig. S1, ESI†) within the PLA host matrix, a visual color change from green to blue was observed with increasing excitation frequencies, where the overall luminescent intensity was found to be dependent on the applied voltage. The ability to incorporate functional materials within 3D printing and additive manufacturing approaches represents a promising direction not only for the future of ACEL devices, but also in the design and development of stimuli-responsive materials, devices, and structures across a diverse range of fields and applications.

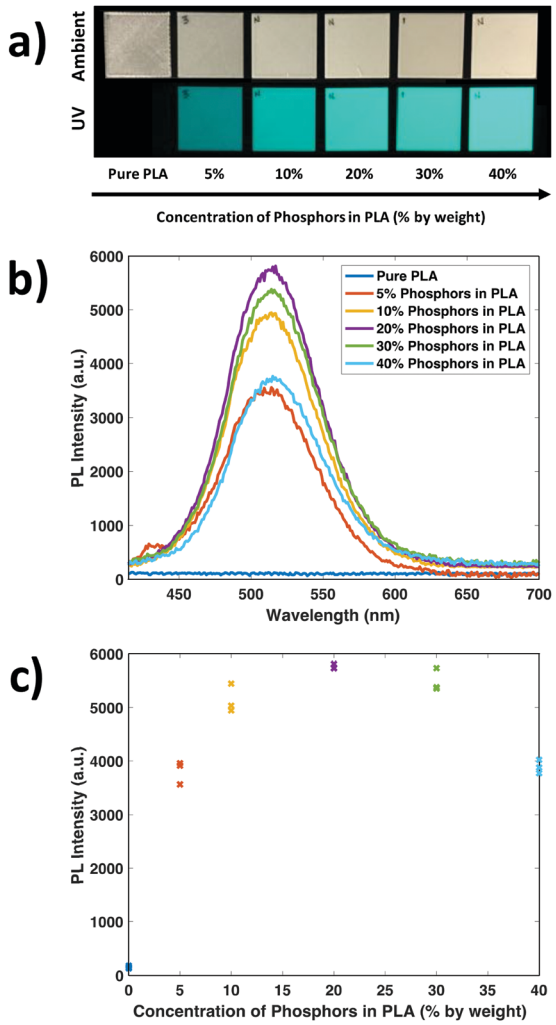

Fig. 1 (a) 3D-printed PLA/phosphor thin film samples at varying concentrations of phosphors in PLA (% by weight) under ambient and UV excitation (top and bottom, respectively); (b) photoluminescence (PL) response of 3D-printed PLA/phosphor thin film samples recorded at varying concentrations of phosphors in PLA (% by weight); and (c) maximum PL intensity for 3D-printed PLA/phosphor thin film samples at varying concentrations of phosphors in PLA (% by weight). Three individual scans for each weight percent are shown in the plot.

Results and discussion

For initial testing, thin film templates, 0.5 mm in thickness, with varying concentrations of embedded phosphors ranging from 5–40% by weight, were fabricated to evaluate the optical response of the PLA/phosphor composite after materials processing and printing. Utilizing a solution-based approach, PLA/phosphor-functionalized filament was fabricated according to established protocols.[24,25] In short, the PLA host matrix and ZnS:Cu phosphor powder were mixed in solvent, dried, shredded, and extruded to manufacture PLA/phosphor filament compatible with conventional FDM type 3D printing systems. A detailed description of the filament fabrication process is included in the ESI.† Thin film samples were printed using a dual nozzle Ultimaker 3 Extended FDM type desktop printer, where functionalized PLA/phosphor filament was extruded through a 0.4 mm nozzle heated to 215 °C, and then deposited at 0.1 mm (100 μm) layer height increments to manufacture the desired structure.

Following printing, PLA/phosphor thin film templates exhibited a bright blue-green luminescent coloration under UV excitation (Fig. 1a). Consistent with other polymer/ZnS:Cu-based phosphor systems,[10] the 3D-printed films exhibited a single monotonic photoluminescence (PL) emissive peak centered near 515 nm (Fig. 1b). Though the overall spectral shape remained constant between the various concentrations tested (Fig. S2, ESI†), the

PL response reached a maximum intensity at a 20% by weight loading of phosphors embedded in PLA (Fig. 1c). We attribute this decrease in PL at higher concentrations to the presence of phosphors in close proximity and a partial wetting of their surface. Though there are more phosphors and subsequent potential light emitting sites, the increased concentration of the surrounding particles effectively reduces the proportion of available light emitting sites, leading to a reduction in PL.[6] Further inspection of the 3D-printed films using differential interference contrast (DIC) microscopy confirms this behavior, where phosphors were observed to exist in close contact with one another, occasionally forming partially aggregated structures in samples containing higher concentrations of embedded phosphors (Fig. S3, ESI†). At a 20% by weight loading, though, phosphors were well dispersed throughout the 3D-printed films, providing a number of light-emitting sites that were observed under WL microscopy (Fig. 2). Based on these findings and observations, all PLA/phosphor samples and ACEL devices were fabricated at a 20% by weight loading of phosphors to maximize the overall luminescent and optical response of the 3D-printed devices and structures.

At 20% by weight, the 3D-printed samples studied in this report were fabricated using a significantly lower concentration of embedded phosphors compared to other ZnS-based devices previously reported in the literature, in which phosphor loadings in excess of 50% by weight are commonly used to obtain the desired optical response and behavior for both electro- and mechano-luminescent applications.[10–13,23] The ability to reduce the overall concentration and required weight of embedded phosphors provides a distinct advantage not only in cost but also in reducing the impact that functionalization has on the underlying material response and behavior of the polymer host matrix. Prior studies have shown that functionalization can impact a number of material properties ranging from mechanical strength and durability and thermal stability.[25–28] By effectively reducing the overall concentration of embedded phosphors needed for device fabrication, we aim to minimize any adverse impacts that functionalization may have on the material properties and response of the PLA host matrix, while still maintaining the optical response necessary to develop functioning ACEL devices.

A schematic representation of the 3D-printed ACEL devices tested in this paper is shown in Fig. 3a. Samples were again fabricated using a dual nozzle Ultimaker 3 Extended FDM type desktop 3D printer, with the same printing parameters used to fabricate the thin film templates discussed earlier. A single layer of PLA/phosphor material (100 μm in thickness) was directly deposited onto a pre-cleaned conductive ITO glass substrate and sandwiched between two layers of 3D-printed conductive carbon-based PLA serving as a second electrode (200 μm in thickness). In total, individual ACEL devices and samples were manufactured in less than 5 minutes, including the time required for nozzle heating and the entire 3D printing process. The optical response of 3D-printed ACEL devices was then evaluated for various frequency- and voltage-dependent excitation conditions using a CCD-based spectrometer system. For each case, a sinusoidal voltage was applied across the single PLA/phosphor layer using a function generator and associated amplification source where samples were tested for voltages ranging from 150 V to 245 V and corresponding frequencies spanning from 10 Hz to 10 kHz.

Still images of a representative 3D-printed ACEL device exposed to a constant voltage source and various excitation frequencies are shown in Fig. 3b. Under these conditions, the 3D-printed samples displayed a bright luminescence that gradually changed color from green to blue with increasing excitation frequencies. The resulting electroluminescent (EL) spectral response was recorded in order to further quantify the impact of voltage and frequency on the optical response and resultant color change for 3D-printed ACEL devices. As the excitation frequency was increased from 300 Hz to 10 kHz under

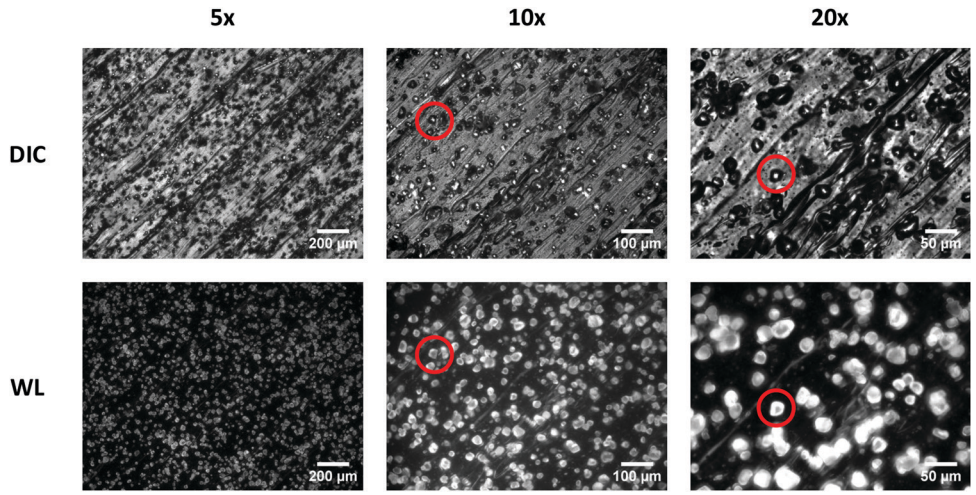

Fig. 2 Differential interference contrast (DIC) and white light (WL) microscopy images for 3D-printed PLA/phosphor thin film samples (20% phosphor in PLA by weight) at increasing levels of magnification. Red circles indicate representative ZnS:Cu phosphor particles embedded in PLA under DIC and WL excitation, respectively. The diagonal lines visible in the images are a result of material deposition and nozzle movement occurring during the 3D printing process and material deposition/sample fabrication.

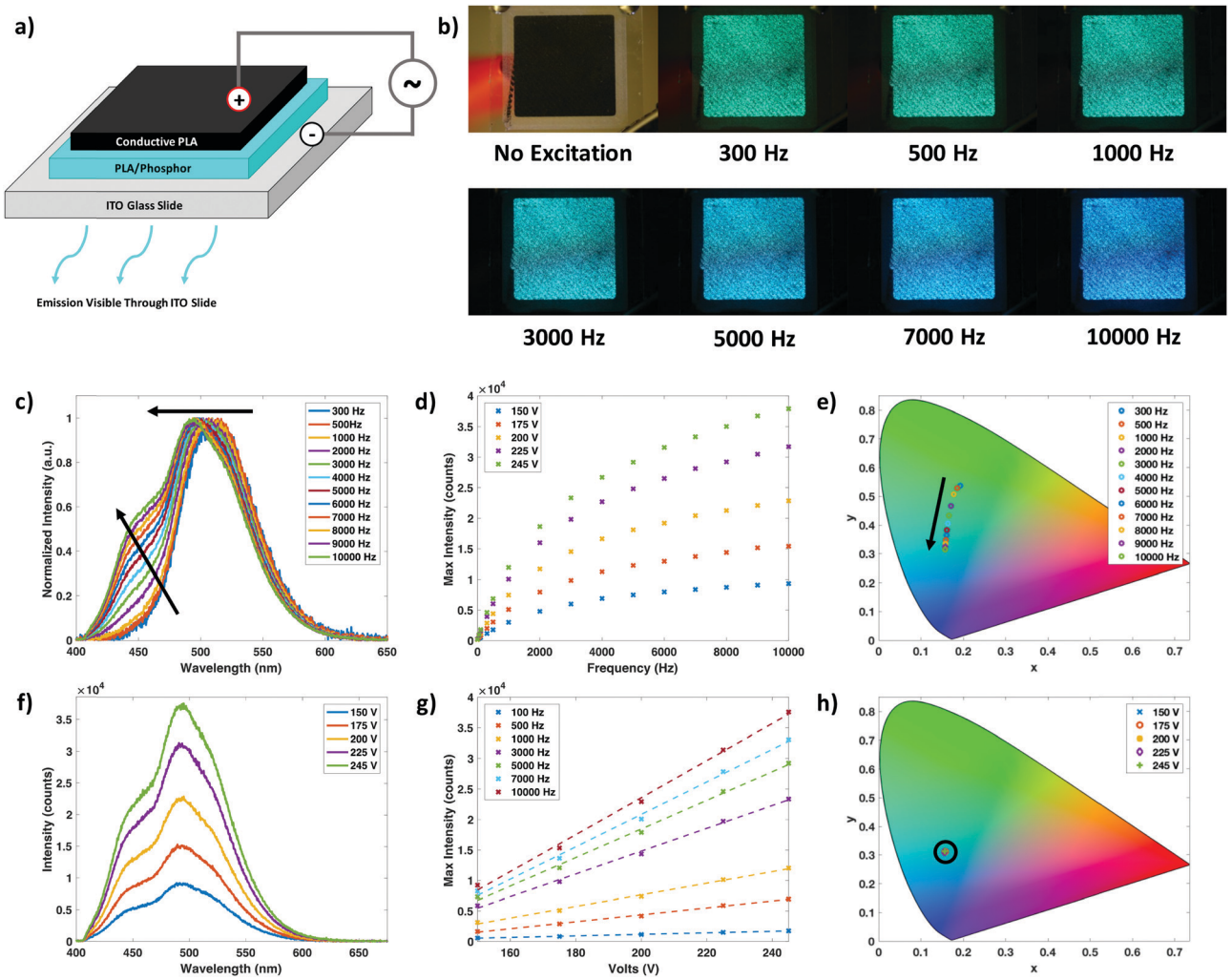

Fig. 3 (a) Schematic representation of 3D-printed ACEL device (from bottom to top: ITO glass slide/3D-printed PLA/phosphor layer (100 μm thickness)/3D-printed conductive PLA electrode (200 μm thickness), where emission is visible through the bottom of the ITO glass slide); (b) still images of 3D-printed ACEL devices at various excitation frequencies under constant applied voltage (245 V); (c) normalized electroluminescence (EL) intensity spectra of a representative ACEL device at increasing frequencies under constant 245 V excitation source (arrows are included as a guide for the eye for increasing frequencies studied); (d) dependence of excitation frequency on maximum PL response at various voltages; (e) CIE coordinate (*x*,*y*) values for EL response at increasing frequencies under 245 V excitation source (arrow is included as a guide for the eye for increasing frequencies studied); (f) representative EL intensity spectra for ACEL device at increasing voltages with a constant 10 kHz excitation source; (g) dependence of excitation voltage on maximum EL response at various frequencies (dashed lines represent linear fits for each frequency studied; additional curve fitting information can be found in the ESI,† Table S3); (h) CIE coordinate (*x*,*y*) values at various voltages for constant 10 kHz excitation source (location of data points for all voltages tested fall within the black circle shown in the figure). EL response of the 3D-printed ACEL devices was found to be stable and reproducible four months after printing and sample fabrication (see Fig. S8, ESI†).

a constant voltage, the maximum EL peak location shifted from 517 nm to 495 nm and a secondary peak emerged near 450 nm for frequencies above 2000 Hz (Fig. 3c). Furthermore, the maximum EL intensity and corresponding brightness of the 3D-printed ACEL devices dramatically increased with increasing frequency (Fig. 3d). Commission Internationale de L'Eclairage (CIE) coordinates were used to visualize the dependence of color and electroluminescence on the applied voltage and excitation frequency by providing a relationship between the recorded spectral response and the corresponding color perceived by the human eye (Fig. 3d). For the representative device shown, the calculated CIE coordinates shifted from (0.19, 0.54) to (0.16, 0.31) when frequency was increased from 300 Hz to 10 kHz, corresponding to the green to blue color change that was visually observed (Fig. 3b). The spectral response and corresponding shifts in both the observed color and in CIE coordinates were consistent among all samples tested, regardless of the applied voltage, where additional information can be found in ESI† (Fig. S4 and S5 and Table S1).

Though the presence of both green and blue emissive bands for ZnS:Cu-based phosphor systems and devices has been well documented,[11] the underlying mechanisms responsible for such spectral response and resultant change in color from green to blue with increasing excitation frequencies remain a topic of debate.

In both cases, researchers hypothesize that the presence of structural impurities and metal dopant substitutions are the primary driving forces behind the optical response. For the green band occurring near 515 nm, a number of research groups attribute this emissive behavior to electron transfer between the impurity-induced shallow donor state arising from sulfur vacancies and the t_2 state of the substituted Cu ions.[11,29–32] An explanation for the subsequent blue emission and shoulder peak occurring near 450 nm, though, has yet to be agreed upon. Conflicting claims attribute blue emission to electron transfer between the native ZnS conduction band and t_2 state of the substituted Cu ions,[29] Zn defect vacancies and resultant trap states not related to Cu dopants,[30] or transitions between sulfur vacancies and the native ZnS valence band.[33,34] With the application of an external voltage source, the recombination of electron–hole pairs between the discrete energy states ultimately leads to the observed blue/green luminescence in our 3D-printed ACEL devices.[18] The contribution of this paper is not to identify the underlying mechanisms driving the emergence of additional emissive peaks with increasing frequency, but rather to demonstrate the capability of developing color tunable ACEL devices using 3D printing and additive manufacturing processes.

The optical response of 3D-printed ACEL devices was also evaluated for voltage-dependent excitation configurations. For a fixed frequency, the recorded EL spectra of a representative 3D-printed ACEL device exposed to various voltage inputs is shown in Fig. 3f. Unlike the results for the frequency-dependent excitation case, the overall shape of the EL spectral response remained unchanged regardless of the applied voltage (Fig. 3f and Fig. S6, ESI†). For this case, the recorded maximum EL intensity and resulting brightness increased as the applied voltage was increased. In fact, for all frequencies tested, the maximum EL intensity was linearly dependent with the applied voltage (Fig. 3g). This response is in agreement with previously reported ACEL devices and can be attributed to an increase in excitation probability where a higher number of electrons are expected to activate more luminescent centers at higher voltages; leading to an increase in EL intensity.[35,36] As the overall EL spectral response and shape remained unchanged with increasing voltages, the recorded CIE coordinates for a fixed excitation frequency also remained constant for all voltages tested (Fig. 3h). The optical response for voltage-dependent excitation was again highly reproducible between individual samples, where additional spectral data can be found in ESI† (Fig. S6 and S7, and Table S2).

When compared to traditional ACEL device fabrication procedures, one of the major benefits of additive manufacturing and 3D printing is the flexibility in the design and manufacturing process. 3D printing provides a number of advantages including reduced production times and minimized material waste. As a potential and relevant application for the work described in this paper, we successfully demonstrated the ability to 3D print individually customized, color tunable, light emitting devices and structures (Fig. 4). Similar to the frequency- and voltage-dependent samples tested, the customized ACEL devices shown in Fig. 4 were 3D printed and manufactured in less than five minutes by depositing a single layer of PLA/phosphor filament onto an ITO slide sandwiched by a conductive PLA top electrode. The luminescent shape and behavior of the ACEL device is controlled by modulating the design of the conductive PLA electrode. When a voltage is applied to the printed device, the ACEL device exhibits luminescent behavior only in regions where the top electrode is in direct contact with the PLA/phosphor layer. Regardless of shape or geometrical configuration, all customized 3D-printed samples displayed a color change from green to blue as the excitation frequency was increased. Using computer aided design (CAD) software, any design, shape, geometry or logo can be incorporated within ACEL devices in a matter of minutes using a 3D printing approach. With the continued advancement of materials development and additive manufacturing technologies, the design of more complex and larger-scale ACEL displays and devices can be realized through the use of additive manufacturing technologies.

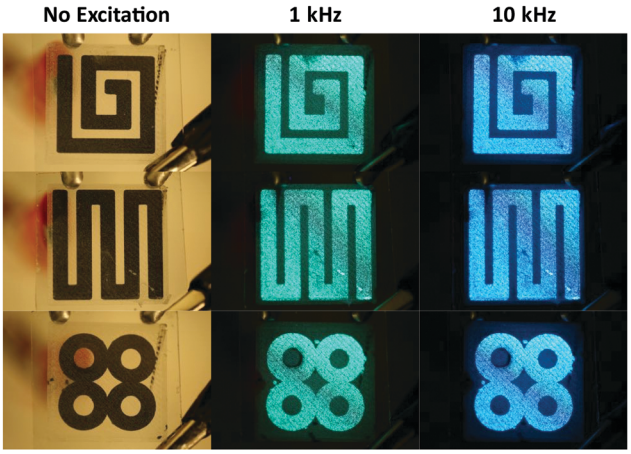

Fig. 4 Demonstration of custom 3D-printed ACEL devices with various geometric patterns under ambient conditions with no excitation, and with a 245 V source under varying excitation frequencies showing visual changes in color.

Conclusions

Through materials design considerations, we have demonstrated the ability to manufacture functional ACEL devices using additive manufacturing and 3D-printing approaches. The luminescent performance and response of 3D-printed PLA/phosphor samples was evaluated at various concentrations, where it was found that a 20%-by-weight loading was the optimal concentration of embedded phosphors in the PLA host matrix. For concentrations above 20%, the luminescent response decreased due to inter-particle interactions within the 3D-printed structure. Individual ACEL devices were fabricated using a FDM approach, where a single layer of PLA/phosphor was directly deposited onto an ITO glass slide and sandwiched between a secondary 3D-printed conductive electrode. When exposed to an external voltage source, 3D-printed ACEL devices exhibited both voltage- and frequency-dependent responses,

where the luminescent color and intensity could be easily modulated. The resultant color of the ACEL device depended exclusively on the applied frequency, where the resultant emission shifted from green to blue as the excitation frequency was increased. When the excitation frequency was held constant, though, the brightness and maximum luminescent intensity were linearly related to the applied voltage for the 3D-printed ACEL devices tested in this study. 3D printing offers an alternative approach to rapidly manufacture ACEL devices and structures and represents a new way of thinking for the continued development of light emitting components and applications across a variety of uses, fields, and industries.

Author contributions

All authors have given approval to the final version of the manuscript.

Funding sources

The Vanderbilt research team would like to acknowledge the support of the U.S. Department of Energy, which provided funding for the project under the support of the Nuclear Energy Enabling Technologies (NEET) Program, Award Number DE-NE0008712.

Conflicts of interest

There are no conflicts of interests to declare.

Acknowledgements

The authors would also like to acknowledge Dr Sandy Rosenthal for access to lab space during the filament fabrication procedure and sample fabrication process.

References

1 B. Allabergenov, H. Shim, H. Y. Noh, M.-J. Lee, H.-K. Lyu, J. Kim and B. Choi, *Adv. Mater. Technol.*, 2017, **2**, 1700040.
2 H. Fang, H. Tian, J. Li, Q. Li, J. Dai, T. L. Ren, G. Dong and Q. Yan, *Nano Energy*, 2016, **20**, 48–56.
3 M. Bredol and H. S. Dieckhoff, *Materials*, 2010, **3**, 1353–1374.
4 B. Hu, D. Li, O. Ala, P. Manandhar, Q. Fan, D. Kasilingam and P. D. Calvert, *Adv. Funct. Mater.*, 2011, **21**, 305–311.
5 C. N. Xu, T. Watanabe, M. Akiyama and X. G. Zheng, *Appl. Phys. Lett.*, 1999, **74**, 1236–1238.
6 S. Krishnan, H. Van der Walt, V. Venkatesh and V. B. Sundaresan, *J. Intell. Mater. Syst. Struct.*, 2017, **28**, 2458–2464.
7 X. Xu, D. Hu, L. Yan, S. Fang, C. Shen, Y. L. Loo, Y. Lin, C. S. Haines, N. Li, A. A. Zakhidov, H. Meng, R. H. Baughman and W. Huang, *Adv. Mater.*, 2017, **28**, 2458–2464.
8 V. Wood, J. E. Halpert, M. J. Panzer, M. G. Bawendi and V. Bulović, *Nano Lett.*, 2009, **9**, 2367–2371.
9 J. H. Park, S. H. Lee, J. S. Kim, A. K. Kwon, H. L. Park and S. Do Han, *J. Lumin.*, 2007, **126**, 566–570.
10 S. M. Jeong, S. Song, S. K. Lee and N. Y. Ha, *Adv. Mater.*, 2013, **25**, 6194–6200.
11 S. Moon Jeong, S. Song, S. K. Lee and B. Choi, *Appl. Phys. Lett.*, 2013, **102**, 51110.
12 V. K. Chandra, B. P. Chandra and P. Jha, *Appl. Phys. Lett.*, 2013, **103**, 161113.
13 S. M. Jeong, S. Song and H. Kim, *Nano Energy*, 2016, **21**, 154–161.
14 X. Wang, H. Zhang, R. Yu, L. Dong, D. Peng, A. Zhang, Y. Zhang, H. Liu, C. Pan and Z. L. Wang, *Adv. Mater.*, 2015, **27**, 2324–2331.
15 Y. Zhang, G. Gao, H. L. W. Chan, J. Dai, Y. Wang and J. Hao, *Adv. Mater.*, 2012, **24**, 1729–1735.
16 C. Larson, B. Peele, S. Li, M. Robinson, L. Beccai, B. Mazzolai and R. Shepherd, *Science*, 2016, **351**, 1071–1074.
17 S. M. Jeong, S. Song, K. Il Joo, J. Kim, S. H. Hwang, J. Jeong and H. Kim, *Energy Environ. Sci.*, 2014, **7**, 3338–3346.
18 L. Chen, M. C. Wong, G. Bai, W. Jie and J. Hao, *Nano Energy*, 2015, **14**, 372–381.
19 S. Jun, Y. Kim, B. K. Ju and J. W. Kim, *Appl. Surf. Sci.*, 2018, **429**, 144–150.
20 N. Terasaki, H. Yamada and C. N. Xu, *Catal. Today*, 2013, **201**, 203–208.
21 X. Wang, C. N. Xu, H. Yamada, K. Nishikubo and X. G. Zheng, *Adv. Mater.*, 2005, **17**, 1254–1258.
22 Z. G. Wang, Y. F. Chen, P. J. Li, X. Hao, J. B. Liu, R. Huang and Y. R. Li, *ACS Nano*, 2011, **5**, 7149–7154.
23 D. K. Patel, B. El Cohen, L. Etgar and S. Magdassi, *Mater. Horiz.*, 2018, **5**, 708–714.
24 C. D. Brubaker, M. A. Davies, J. R. McBride, S. J. Rosenthal, G. Kane Jennings and D. E. Adams, *ACS Appl. Nano Mater.*, 2018, **1**, 1377–1384.
25 C. D. Brubaker, T. M. Frecker, J. R. McBride, K. R. Reid, G. K. Jennings, S. J. Rosenthal and D. E. Adams, *J. Mater. Chem. C*, 2018, **6**, 7584–7593.
26 J. H. Lee, P. Zapata, S. Choi and J. C. Meredith, *Polymer*, 2010, **51**, 5744–5755.
27 A. Bansal, H. Yang, C. Li, K. Cho, B. C. Benicewicz, S. K. Kumar and L. S. Schadler, *Nat. Mater.*, 2005, **4**, 693–698.
28 B. J. Ash, R. W. Siegel and L. S. Schadler, *Macromolecules*, 2004, **37**, 1358–1369.
29 S. J. Xu, S. J. Chua, B. Liu, L. M. Gan, C. H. Chew and G. Q. Xu, *Appl. Phys. Lett.*, 1998, **73**, 478–480.
30 W. Q. Peng, G. W. Cong, S. C. Qu and Z. G. Wang, *Opt. Mater.*, 2006, **29**, 313–317.
31 R. Sreeja, K. Sridharan, R. Philip and M. K. Jayaraj, *Opt. Mater.*, 2014, **36**, 861–866.
32 H. Fang, H. Tian, J. Li, Q. Li, J. Dai, T. L. Ren, G. Dong and Q. Yan, *Nano Energy*, 2016, **20**, 48–56.
33 G. Murugadoss, *Particuology*, 2013, **11**, 566–573.
34 S. Ummartyotin, N. Bunnak, J. Juntaro, M. Sain and H. Manuspiya, *Solid State Sci.*, 2012, **14**, 299–304.
35 S. Jun, Y. Kim, B. K. Ju and J. W. Kim, *Appl. Surf. Sci.*, 2018, **429**, 144–150.
36 B. Qiao, Z. L. Tang, Z. T. Zhang and L. Chen, *Mater. Lett.*, 2007, **61**, 401–404.

